NANO LETTERS
Cite This: Nano Lett. 2019, 19, 203−209
Letter
pubs.acs.org/NanoLett

Exosome-like Nanozyme Vesicles for H_2O_2-Responsive Catalytic Photoacoustic Imaging of Xenograft Nasopharyngeal Carcinoma

Hui Ding,[†,‡,§,¶] Yanjuan Cai,[†,§] Lizeng Gao,[⊥] Minmin Liang,[‡] Beiping Miao,[†,§] Hanwei Wu,[†,§] Yang Liu,[†] Ni Xie,[†] Aifa Tang,[†] Kelong Fan,[*,‡] Xiyun Yan,[*,‡] and Guohui Nie[*,†,§]

[†]Institute of Translational Medicine, Shenzhen Second People's Hospital, The First Affiliated Hospital of Shenzhen University, Health Science Center, Shenzhen 518039, China

[‡]Key Laboratory of Protein and Peptide Pharmaceuticals, CAS-University of Tokyo Joint Laboratory of Structural Virology and Immunology, Institute of Biophysics, Chinese Academy of Sciences, Beijing 100101, China

[§]Department of Otolaryngology, Shenzhen Second People's Hospital, The First Affiliated Hospital of Shenzhen University, Shenzhen 518039, China

[⊥]Department of Pharmacology, School of Medicine, Institute of Translational Medicine, Yangzhou University, Yangzhou 225001, China

[¶]The First Affiliated Hospital of Sun Yat-Sen University, Guangzhou 510080, China

Supporting Information

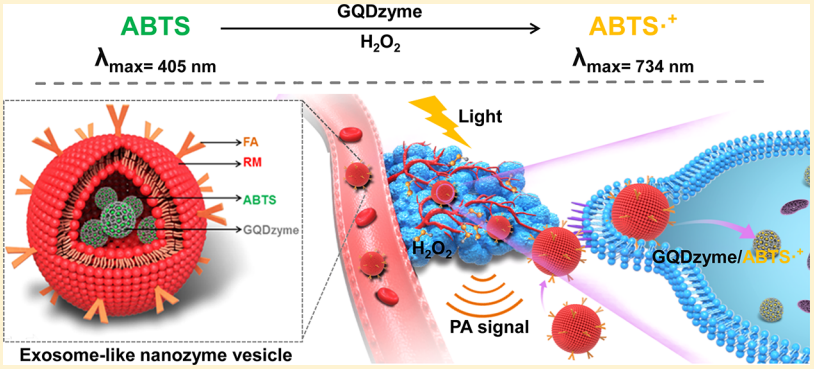

ABSTRACT: Photoacoustic imaging (PAI) is an attractive imaging modality, which is promising for clinical cancer diagnosis due to its advantages on deep tissue penetration and fine spatial resolution. However, few tumor catalytic/responsive PAI strategies are developed. Here, we design an exosome-like nanozyme vesicle for *in vivo* H_2O_2-responsive PAI of nasopharyngeal carcinoma (NPC). The intrinsic peroxidase-like activity of graphene quantum dot nanozyme (GQDzyme) effectively converts the 2,2′-azino-*bis* (3-ethylbenzothiazoline-6-sulfonic acid) (ABTS) into its oxidized form in the presence of H_2O_2. The oxidized ABTS exhibits strong near-infrared (NIR) absorbance, rendering it to be an ideal contrast agent for PAI. Thus, GQDzyme/ABTS nanoparticle is a novel type of catalytic PAI contrast agent, which is sensitive to H_2O_2 produced from NPC cells. Furthermore, we develop an approach to construct exosome-like nanozyme vesicle via biomimetic functionalization of GQDzyme/ABTS nanoparticle with natural erythrocyte membrane modified with folate acid. *In vivo* animal experiments demonstrated that this exosome-like nanozyme vesicle effectively accumulated in NPC and selectively triggered catalytic PAI for NPC. In addition, our nanozyme vesicle exhibits excellent biocompatibility and stealth ability for long blood circulation. Together, we demonstrate that GQDzyme/ABTS based exosome-like nanozyme vesicle is an ideal nanoplatform for developing deep-tissue tumor-targeted catalytic PAI *in vivo*.

KEYWORDS: *Photoacoustic imaging, H_2O_2-responsive, graphene quantum dot nanozyme, exosome-like vesicle, erythrocyte membranes, nasopharyngeal carcinoma*

Nanozymes have gained tremendous attention for their promising potentials for biomedical applications. So far, increasing numbers of nanomaterials have been found to possess intrinsic enzymatic activity similar to natural enzymes such as catalase, glucose oxidases, oxidases, peroxidases, haloperoxidases, superoxide dismutases, and sulfite oxidases.[1−3] A pioneer in these nanomaterials is GQDzyme (a nanometer-sized fragments of graphene), which has shown several advantages in biomedical applications due to its intrinsic peroxidase-like activity, unique structural, and better

Received: September 13, 2018
Revised: December 11, 2018
Published: December 12, 2018

DOI: 10.1021/acs.nanolett.8b03709
Nano Lett. 2019, 19, 203−209

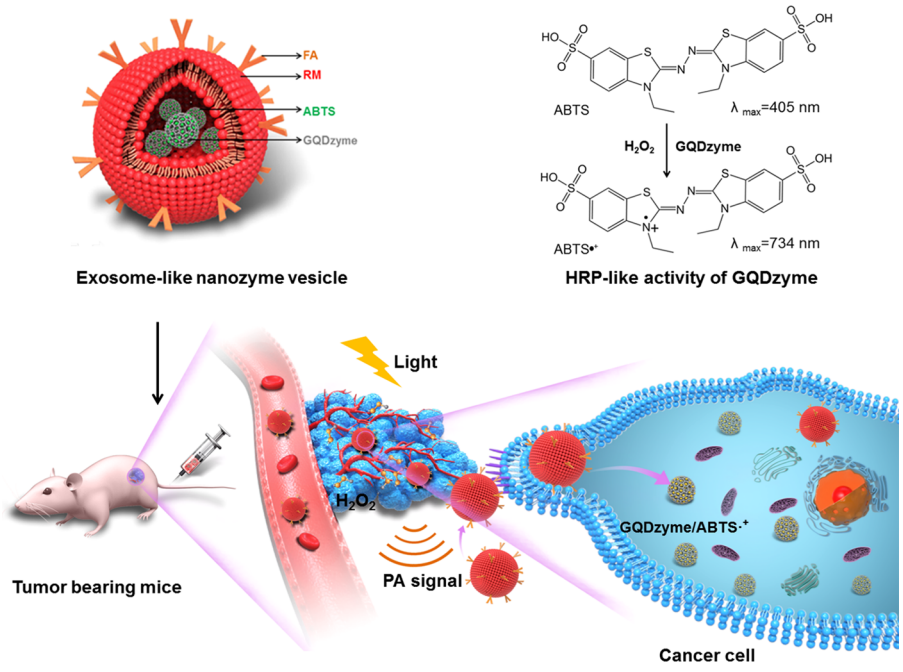

Figure 1. Schematic illustration of exosome-like nanozyme vesicles for catalytic photoacoustic imaging of NPC tumors.

surface grafting using $\pi-\pi$ conjugation.[4−11] Here, we report that GQDzyme can serve as an efficient and stable nanozyme for *in vivo* photoacoustic imaging (PAI).

With catalytic behavior similar to natural horseradish peroxidase (HRP), GQDzyme possesses great potential for H_2O_2 detection. In living organisms, H_2O_2 is the most stable compound of the reactive oxygen species and acts as signaling molecule and plays a crucial role in cell growth, proliferation, and differentiation. In particular, the high levels of H_2O_2 commonly observed in cancer cells may be essential for cancer development.[12,13] The generation and alternation of cellular H_2O_2 have been demonstrated to connect with several physiological and pathological processes of cancer including cell proliferation, apoptosis resistance, and metastasis. Therefore, accurately determining the H_2O_2 level in tumor is of paramount importance and represents a challenge for diagnosis and treatment of tumor. Compared with traditional small molecular tracers for H_2O_2 detection, one of the main advantages of nanozyme probes is the ultrasensitive detection at the relatively low concentrations of H_2O_2 in specific physiological environments.[6,14]

With the advances in tumor visualization, there has been a growing interest in H_2O_2-responsive PAI nanosensors, as there are presence of substantial amount of H_2O_2 in the tumor microenvironment. The underlying principle of PAI is that the contrast agent in biological specimen absorbs the pulsed laser radiation energy and converts it into acoustic signal, which is measured and visualized as an image by a scanning transducer.[15] Thus, multifunctional nanomaterials, which are engineered to possess optimal absorption in the near-infrared (NIR) with very high cross-sections, contribute to PAI applications when these nanomaterials used as PAI contrast agents with sensitivities in the range of low-picomolar concentrations.[8,16−18] On the basis of the above-mentioned view, GQDzyme may serve as a promising PAI contrast agent. In the presence of H_2O_2, GQDzyme is able to convert ABTS into oxidized ABTS with strong NIR absorbance, which potentially can be applied as an ideal contrast agent in PAI of tumors.[14,19] Moreover, the acidic microenvironment in tumors facilitates H_2O_2-responsive PAI imaging through peroxidase-like activity of nanozymes.

NPC, which arises from the epithelium of the nasopharyngeal mucosa associated with latent Epstein−Barr virus infection in most cases, is one type of head and neck cancer in southern Asia, southern China, North Africa, and Alaska. Long-term survival rates differ substantially between patients with early stage NPC (stages I and II) and advanced-stage (stages III and IV). The relative four-year survival rates of patients diagnosed with NPC in stages early stage and advanced-stage are 96.7% and 67.1%, respectively.[20,21] Therefore, early diagnosis is the bottleneck and key to conquer this cancer. PAI with deep tissue imaging ability could provide an efficient diagnostic approach for NPC diagnosis.

To construct an ideal NPC-responsive nanozyme catalytic PAI agents, we employed GQDzyme and its substrates ABTS as components of agents. The oxidized ABTS exhibits strong NIR absorbance, rendering it to be an ideal contrast agent for PAI. By decorating the ABTS on the surface of GQDzyme, we developed a unique and robust H_2O_2-triggered nanozyme catalytic PAI contrast agent. Inspired by exosome, which is cell-extruded membranous bioactive vesicle, we construct an exosome-like nanozyme vesicle by camouflaging GQDzyme/ABTS nanoparticles with folate acid (FA) conjugated natural erythrocyte membranes (RM). Our nanozyme vesicles are able to sensitively detect the relative increased H_2O_2 in NPC as compared to normal tissues due to the rapid metabolism of tumors. In addition, the exosome-like nanozyme vesicle shows superior stealth ability, enhanced circulation time, and improved accumulation in tumors.[22,23] The NPC targeting ability of nanozyme vesicle is achieved by conjugating FA onto the surface of the nanozyme vesicle to target folate receptor (FR) that are overexpressed in NPC cells.[21,24] The H_2O_2-responsvie catalytic PAI imaging ability of exosome-like nanozyme vesicle was investigated via an *in vivo* image test on NPC-bearing mice and the markedly improved PAI efficacy was confirmed. This work is the first demonstration of

DOI: 10.1021/acs.nanolett.8b03709
Nano Lett. 2019, 19, 203−209

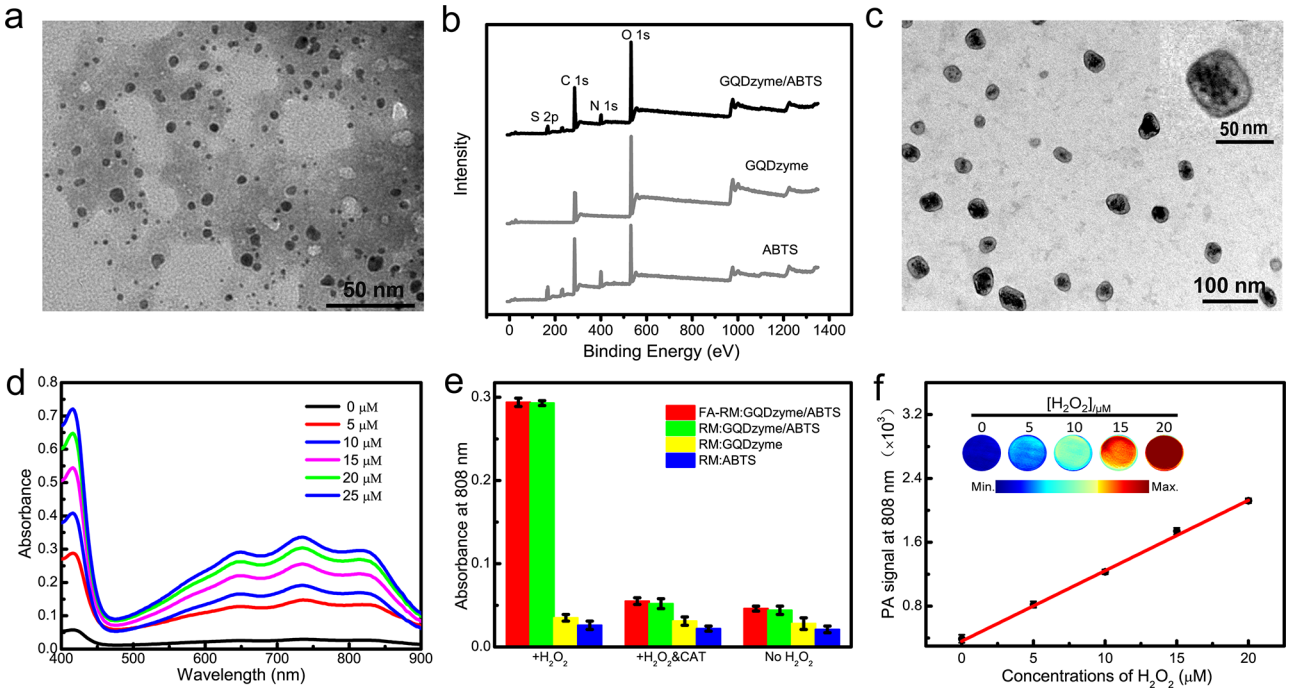

Figure 2. Characterization of exosome-like nanozyme vesicles for PAI. (a) TEM image of GQDzyme/ABTS. (b) XPS analysis of ABTS, GQDzyme, and GQDzyme/ABTS. (c) TEM image of RM:GQDzyme/ABTS. (d) Fluorescence emission spectra of FA-RM:GQDzyme/ABTS at NIR region after incubation with various concentrations of H_2O_2. (e) Absorbance of FA-RM:GQDzyme/ABTS at 808 nm in the presence of H_2O_2, H_2O_2 pretreated with Cat, and no H_2O_2 as a function of incubation time at 37 °C. (f) Linear relationship analysis of correlation between PA signal intensity and concentration of FA-RM:GQDzyme/ABTS. Inset: PAI phantoms consisting of various concentrations of H_2O_2 embedded in agar gel cylinders.

nanozymes based catalytic imaging strategy applied in PAI *in vivo* (Figure 1).

To prepare GQDzyme/ABTS nanoparticles, GQDzyme was synthesized through a facile chemical oxidation and exfoliation method using polyacrylonitrile carbon fibers as the raw material. As shown in Figure S1, GQDzyme exhibited typical Michaelis−Menten kinetics in the ABTS colorimetric reaction. The apparent affinity (K_M) of the GQDzyme for H_2O_2 is comparable with that of nature peroxidase HRP,[25] which warrant the effective catalytic reaction *in vivo*. The GQDzyme was then loaded with its substrate ABTS via $\pi-\pi$ interaction mechanism. Transmission electron microscopy (TEM) characterization showed that the obtained GQDzyme/ABTS were typically ∼10 nm in size with a relatively narrow polydispersity (Figure 2a). The successful loading of ABTS onto the surface of GQDzyme is verified by photoelectron spectroscopy (XPS) analysis (Figure 2b). The sulfur XPS signal further verified the conjugation of ABTS on GQDzyme. In addition, the loading effciency of ABTS was determined to be 64.5% via HPLC with UV detection at 280 nm.

To obtain exosome-like GQDzyme/ABTS nanoparticles, purified natural RM was first extracted from red blood cells using the method reported by Zhang et al.[26−29] TEM characterization of these PAI agents, denoted as RM:GQDzyme/ABTS, exhibited their spherical shapes with the cloaked RM layer with an average nanoparticle size of 40 nm (Figure 2c). As in our previous work,[7,30,31] DSPE-PEG_{2000}-FA ligand was decorated on the RM surface during the process of extrusion. As measured by dynamic light scattering (DLS), the slightly increased particle size and zeta potential also indicated the success of the FA anchoring on the membrane surface. Finally, DLS measurement of the FA-RM:GQDzyme/ABTS reported an average hydrodynamic radius of ∼50 nm (Figure S2) and a narrow polydispersity less than 0.1 (Table S1).

The natural peroxidase enzyme horseradish peroxidase (HRP) has been reported to catalyze the oxidation of ABTS in the presence of environmental H_2O_2 into its oxidized form in the application of photoacoustic inflammation imaging and tumor theranostics. Possessing HRP-like activity, GQDzyme can catalyze the reaction of the ABTS in the presence of H_2O_2. The oxidized ABTS exhibit the major characteristic absorption peaks at 808 nm. In addition, the oxidation reaction rate of ABTS was markedly improved with increasing H_2O_2 concentration in the range from 5 μM to 25 μM (Figure 2d). Moreover, the absorption in NIR region of FA-RM:GQDzyme/ABTS without H_2O_2 was not detected (Figure 2e). RM:GQDzyme and RM:ABTS with or without H_2O_2 showed no obviously NIR absorbance at 808 nm. In contrast, FA-RM:GQDzyme/ABTS and RM:GQDzyme/ABTS incubated with H_2O_2 showed obviously increased NIR absorbance. The NIR absorbance of FA-RM:GQDzyme/ABTS was significantly suppressed when the H_2O_2 was pretreated by catalase (Cat), which triggers the decomposition of H_2O_2. These results confirm that GQDzyme possesses the peroxidase-like activity and the nanozyme vesicles system is selectively activated when the H_2O_2 presents.

To assess their potential for *in vitro* PAI, FA-RM:GQDzyme/ABTS incubated with various H_2O_2 concentrations in solutions were embedded in agar gel cylinders to tested the PA signals. Figure 2f showed that the detected PA signals were markedly increased with the higher H_2O_2 concentration. More importantly, a good correlation between PA signals and H_2O_2 concentration was confirmed. On the

DOI: 10.1021/acs.nanolett.8b03709
Nano Lett. 2019, 19, 203−209

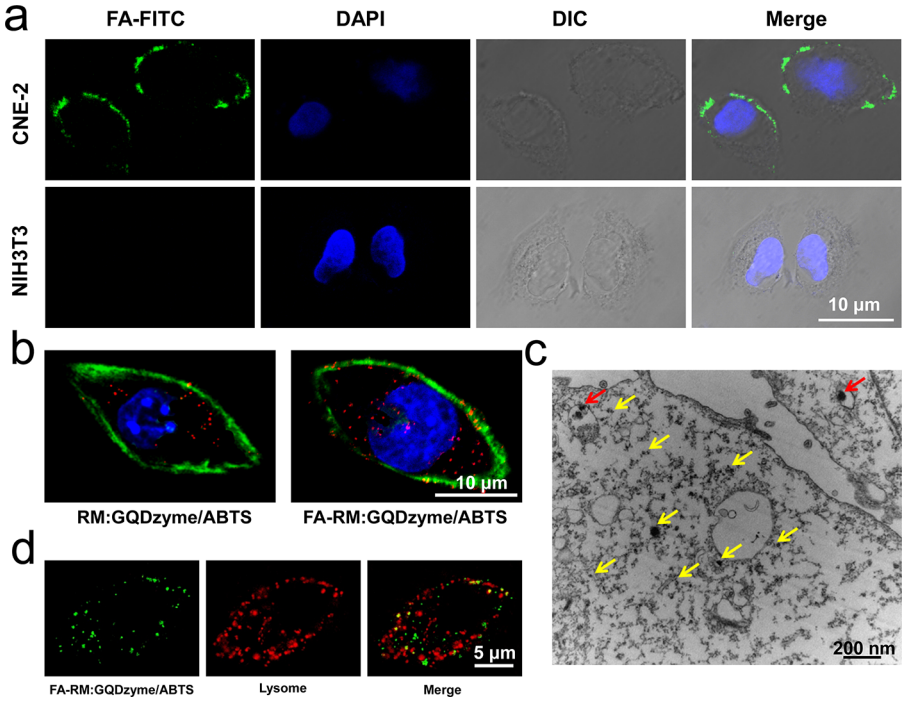

Figure 3. Specific binding of exosome-like nanozyme vesicles to NPC tumor cells and subcellular localization of nanozyme vesicles in tumor cells. (a) FR expression on CNE-2 cells compared with FR-negative NIH3T3 cells, and the corresponding CLSM images. (b) CLSM images of internalization by CNE-2 cell (red spots indicate nanozyme vesicles, blue indicates cell nucleus, and green indicates cell membrane). (c) TEM image of CNE-2 cells treated with FA-RM:GQDzyme/ABTS. (d) CLSM images of lysosomes in CNE-2 cells with internalized FA-RM:GQDzyme/ABTS nanoparticles (red arrows indicate the colocalization nanoparticles, and yellow arrows indicate the nonlocalization nanoparticles).

basis of a linear regression analysis as illustrated in Figure 2f, a correlation coefficient R^2 = 0.9699 was eventually obtained. The GQDzyme/ABTS exhibited good stability in agar gel cylinders during the observed 48 h, with a few changes in the PA signal intensity, especially in RM-coated groups (Figure S3). The excellent stability of GQDzyme/ABTS and FA-RM:GQDzyme/ABTS enables their pharmacokinetic activities *in vivo*. Moreover, as shown in Figure S4, the half-life of GQDzyme/ABTS in circulation was only 6 h, while those of exosome-like GQDzyme/ABTS nanoparticles groups were markedly increased (>24 h). The pharmacokinetic profiles of GQDzyme/ABTS, RM:GQDzyme/ABTS, and FA-RM:GQDzyme/ABTS further demonstrated that RM could greatly prolong the circulation time in the bloodstream. These results verify that FA-RM:GQDzyme/ABTS possesses the potential to act as an ideal contrast agent for PAI.

To efficiently amass in the lesion site, nanoparticles should possess high specific binding affinity toward tumor cells. In this work, FA was conjugated onto RM-coated nanoparticles with high payload for NPC-targeted nanocarrier-based delivery. As shown in confocal laser scanning microscopy (CLSM) imaging (Figure 3a), FA-FITC bound preferentially to the FR, which is a membrane-associated folate binding protein highly expressed on the surface of CNE-2 cells when compared with FR-negative NIH3T3 cells. Fluorescent signal of FITC strongly presented in the group of NPC cell line CNE-2 cells, but no signal in NIH3T3 cells. As expected, comparing with nanozyme vesicles, the cellular uptake of FA-nanozyme vesicles was significantly promoted with the assistance of folate targeting (Figure 3b). Moreover, RM cloaking and FA targeting induced the membrane fusion process and helped the nanozyme/ABTS nanoparticles escape from the lysosome. When FA-RM:GQDzyme/ABTS nanoparticles encounter cancer cells, the lateral diffusion of the cell membrane enables the formation of a preferred static pattern for the recognition, which has been widely found during cell−cell interaction. Such a spatial organization from anisotropy to isotropy generates multivalent driving forces between folate acid and folate receptor, which would trigger the membrane fusion process. Therefore, most FA-RM:GQDzyme/ABTS could directly penetrate into the cytoplasm (not escape from endosomes/lysosome). The nanozyme vesicles were detected in the cytoplasm as seen from Figure 3c and 3d with low lysosome colocalization ratio, which allowed the encapsulated GQDzyme/ABTS to be directly released into the cytoplasm. Thus, nanozyme vesicles with lysosomal escape ability facilitated the interactions of GQDzyme/ABTS nanoparticles with cell membrane, mitochondria, and peroxisome, which generated hydrogen peroxide and superoxide anions, resulting in producing abundant PAI contrasts. We also evaluated the safety of FA-RM:GQDzyme/ABTS by measuring cell viability with CCK-8 kit. As shown in Figure S5, only a little cytotoxicity was detected when CNE-2 cells were treated with FA-RM:GQDzyme/ABTS suggesting the excellent biosafety of PAI contrast agent.

The above promising results led us to test the feasibility of exosome-like nanozyme vesicles used as a H_2O_2-responsive PAI for NPC diagnosis *in vivo*. On the basis of our previous work, we have confirmed that camouflaging with RM greatly prolonged the circulating time in blood of the nanoparticles and endow nanoparticles with satisfactory stealth performance to escape the entrapment of RES, resulting in efficient accumulation at tumor sites. In this paper, nanozyme vesicles FA-RM:GQDzyme/ABTS were injected intravenously into

DOI: 10.1021/acs.nanolett.8b03709
Nano Lett. 2019, 19, 203−209

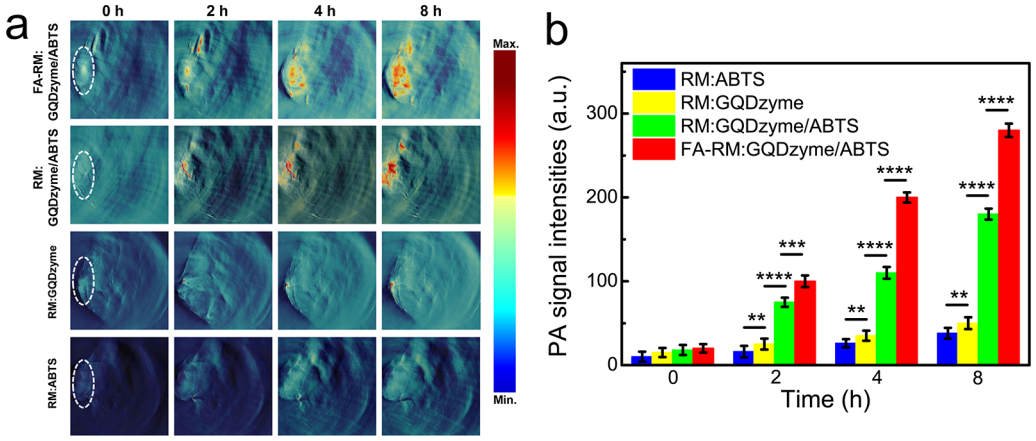

Figure 4. *In vivo* H_2O_2-responsive PAI for NPC detection with exosome-like nanozyme vesicles. (a) PAI of tumor in nude mice before and 2, 4, and 8 h intravenous postinjections of nanozyme vesicles. (b) Average PA signal intensity of tumor tissues of panel a. Error bars represent the standard deviations (n = 3). $^{**}p < 0.01$, $^{***}p < 0.001$, $^{****}p < 0.0001$.

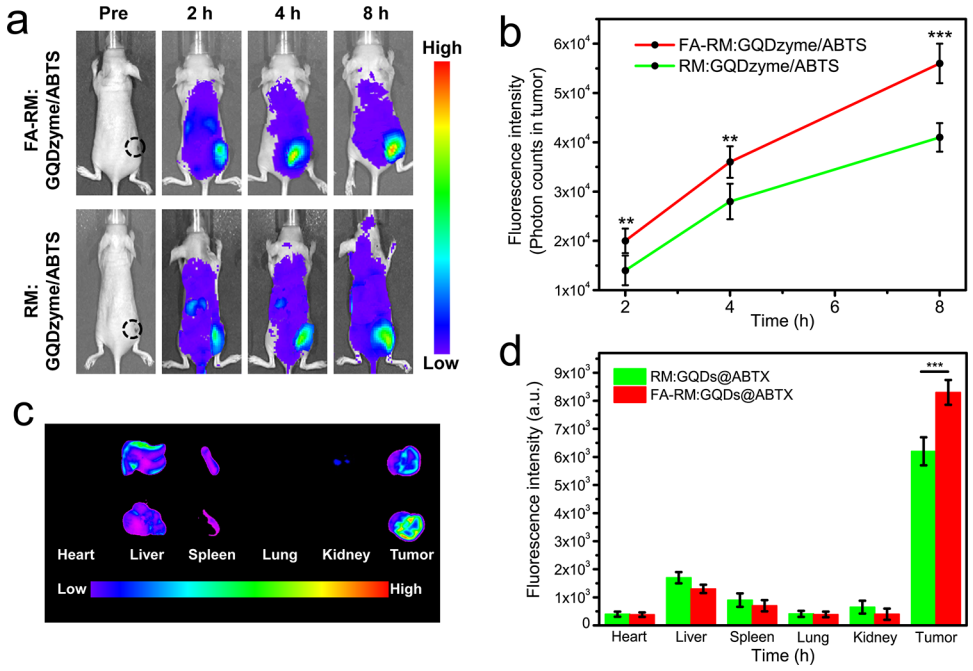

Figure 5. *In vivo* fluorescence images of exosome-like nanozyme vesicles in NPC tumor-bearing mice after intravenous injection. a) NIR fluorescence images of CNE-2 tumor-bearing mice at 1, 3, and 6 h after intravenous injection of nanozyme vesicles. b) NIR fluorescence signal intensity in tumor region. c) Representative *ex vivo* fluorescence images of the tumors and main organs of CNE-2-bearing mice sacrificed at 48 h after intravenous injection of nanozyme vesicles: RM:GQDzyme/ABTS (top) and FA-RM:GQDzyme/ABTs (bottom). d) Tissue distribution in CNE-2-bearing mice after treatment with the different nanozyme vesicles for 48 h. $^{**}p < 0.01$, $^{***}p < 0.001$.

mice bearing CNE-2 tumor to realize PA image. As shown in Figure 4a, the PA signal was clearly visualized and gradually increased in the CNE-2 tumor in both FA-RM:GQDzyme/ABTS and RM:GQDzyme/ABTS treated groups. The PA signal at the tumor site was detected as early as 2 h after the injection. Moreover, the *in vivo* tumor PA signal markedly and continuously increased with time, resulting in a signal 10 times stronger than its counterpart 8 h after the injection (Figure 4b). In addition, intravenous injection of FA-RM:GQDzyme/ABTS in mice led to a higher photoacoustic signal in the tumor compared with mice injected with RM:GQDzyme/ABTS, confirming the enhanced tumor targeting ability by modification of FA. However, in the RM:GQDzyme group, a little of PA signal was also detected, due to the superior mechanical and thermal properties of RM:GQDzyme. The naked GQDzyme/ABTS barely accumulated in the tumor sites because of their poor stealth property and their absence of tumor targeting ability (Figure S6). RM:ABTS without GQDzyme exhibited no PA signal coincided with the experimental results *in vitro*. In addition, we replaced ABTS with a fluorescent DIR dye and then further evaluated the time-elapsed biodistribution of the agents with FA after intravenous injection. Results indicated that FA-RM:GQDzyme/ABTS efficiently accumulated at tumor sites (Figure 5a and 5b). In addition, the data shown in Figure 5c and in corresponding quantitative data in Figure 5d further demonstrated the excellent delivery performance of these nanozyme vesicles. The naked GQDzyme/ABTS mainly accumulated in the liver, spleen, and kidney within 48 h because of their poor stealth property (Figure S7). Moreover,

DOI: 10.1021/acs.nanolett.8b03709
Nano Lett. 2019, 19, 203−209

no obvious toxicities or inflammatory infiltrates were observed in the histological sections of heart, liver, spleen, lung, and kidney (Figure S8), which further confirmed the safety of FA-RM:GQDzyme/ABTS, indicating that our nanozyme vesicles possess good biocompatibility.

In summary, we have developed a novel H_2O_2-responsive exosome-like nanozyme vesicle for NPC PAI detection. This nanozyme vesicle consisted of GQDzyme/ABTS nanoparticles coated with isolated RM decorated by FA targeting moiety to mimic the exosome compartmentalization strategy for PAI of NPC. This biomimetic decoration contributes to the prolonging circulation time, improving tumor accumulation, and facilitating tumor uptake, which were superior to those exhibited by the traditional nonbiological materials modification strategies. Importantly, the lysosomal escape ability of our exosome-like nanozyme vesicles facilitates the interactions of nanozyme and H_2O_2-producing organelles. Meanwhile, on the basis of GQDzyme with peroxidase-like activity, PA signal is enhanced in the tumor H_2O_2 environment owing to the optical absorption and photothermal properties of nanozyme' substrates ABTS. In addition to loading ABTS in PAI, GQDzyme functions as nanocarriers for tracking and delivery of drugs as previously reported. Overall, FA-RM:GQDzyme/ABTS is potentially exploited as H_2O_2-responsive photoacoustic contrast agents to noninvasively image NPC and other types of tumors. The versatility of this strategy can fulfill the research and clinic need of cancer diagnosis.

■ ASSOCIATED CONTENT

Supporting Information

The Supporting Information is available free of charge on the ACS Publications website at DOI: 10.1021/acs.nanolett.8b03709.

Detailed experimental materials and synthesis strategies, additional characterizations methods and results of GQDzymes, pharmacokinetic profile study, stability evaluations of PA signal intensity, *in vivo* fluorescence images of nanozyme vesicles and related HE staining analysis (PDF)

■ AUTHOR INFORMATION

Corresponding Authors

*E-mail: fankelong@ibp.ac.cn. Phone: +86-10-64888256.
*E-mail: yanxy@ibp.ac.cn. Phone: +86-10-64888583.
*E-mail: nghui@21cn.com. Phone: +86-755-83366388.

ORCID

Kelong Fan: 0000-0001-6285-1933
Xiyun Yan: 0000-0002-7290-352X

Notes

The authors declare no competing financial interest.

■ ACKNOWLEDGMENTS

This work was supported by Sanming Project of Medicine in Shenzhen (SZSM201612031), China Postdoctoral Science Foundation (2018M633229), Natural Science Foundation of Guangdong Province (2018A030310665, 2018A0303130295), National Natural Science Foundation of China (No. 31530026, 31871005), the Strategic Priority Research Program (Grant No. XDB29040101) of CAS, Young Elite Scientist Sponsorship Program by CAST (2015QNRC001), and Shenzhen Science and Technology Innovation Committee (JCYJ20170306091657539, JCYJ20170413162242627, JCYJ20170306091452714, GJHZ20170313172439851).

■ REFERENCES

(1) Gao, L.; Zhuang, J.; Nie, L.; Zhang, J.; Zhang, Y.; Gu, N.; Wang, T.; Feng, J.; Yang, D.; Perrett, S. *Nat. Nanotechnol.* **2007**, *2* (9), 577−583.
(2) Wei, H.; Wang, E. *Chem. Soc. Rev.* **2013**, *42* (14), 6060−6093.
(3) Fan, K.; Xi, J.; Fan, L.; Wang, P.; Zhu, C.; Tang, Y.; Xu, X.; Liang, M.; Jiang, B.; Yan, X. *Nat. Commun.* **2018**, *9* (1), 1440 DOI: 10.1038/s41467-018-03903-8.
(4) Lin, L.; Song, X.; Chen, Y.; Rong, M.; Zhao, T.; Wang, Y.; Jiang, Y.; Chen, X. *Anal. Chim. Acta* **2015**, *869*, 89−95.
(5) Song, Y.; Qu, K.; Zhao, C.; Ren, J.; Qu, X. *Adv. Mater.* **2010**, *22* (19), 2206−2210.
(6) Smith, B. R.; Gambhir, S. S. *Chem. Rev.* **2017**, *117* (3), 901−986.
(7) Ding, H.; Zhang, F.; Zhao, C.; Lv, Y.; Ma, G.; Wei, W.; Tian, Z. *ACS Appl. Mater. Interfaces* **2017**, *9* (33), 27396.
(8) De La Zerda, A.; Zavaleta, C.; Keren, S.; Vaithilingam, S.; Bodapati, S.; Liu, Z.; Levi, J.; Smith, B. R.; Ma, T. J.; Oralkan, O.; et al. *Nat. Nanotechnol.* **2008**, *3* (9), 557−62.
(9) Yoo, J. M.; Kang, J. H.; Hong, B. H. *Chem. Soc. Rev.* **2015**, *44* (14), 4835−52.
(10) Sun, H.; Gao, N.; Dong, K.; Ren, J.; Qu, X. *ACS Nano* **2014**, *8* (6), 6202−6210.
(11) Liu, M.; Zhao, H.; Chen, S.; Yu, H.; Quan, X. *ACS Nano* **2012**, *6* (4), 3142.
(12) Zhang, Y.; Wu, C.; Zhou, X.; Wu, X.; Yang, Y.; Wu, H.; Guo, S.; Zhang, J. *Nanoscale* **2013**, *5* (5), 1816−1819.
(13) Molinaro, R.; Corbo, C.; Martinez, J. O.; Taraballi, F.; Evangelopoulos, M.; Minardi, S.; Yazdi, I. K.; Zhao, P.; Rosa, E. D.; Sherman, M.; et al. *Nat. Mater.* **2016**, *15* (9), 1037−1046.
(14) Kim, K.; Kim, J. H.; Park, H.; Kim, Y. S.; Park, K.; Nam, H.; Lee, S.; Park, J. H.; Park, R. W.; Kim, I. S. *J. Controlled Release* **2010**, *146* (2), 219−227.
(15) Chen, Q.; Liang, C.; Sun, X.; Chen, J.; Yang, Z.; Zhao, H.; Feng, L.; Liu, Z. *Proc. Natl. Acad. Sci. U. S. A.* **2017**, *114* (21), 5343.
(16) Chen, Q.; Liu, X.; Chen, J.; Zeng, J.; Cheng, Z.; Liu, Z. *Adv. Mater.* **2015**, *27* (43), 6820−6827.
(17) Li, K.; Liu, B. *Chem. Soc. Rev.* **2014**, *43* (18), 6570−6597.
(18) Pu, K.; Shuhendler, A. J.; Jokerst, J. V.; Mei, J.; Gambhir, S. S.; Bao, Z.; Rao, J. *Nat. Nanotechnol.* **2014**, *9* (3), 233−239.
(19) Yang, W.; Guo, W.; Le, W.; Lv, G.; Zhang, F.; Lei, S.; Wang, X.; Wang, J.; Sheng, W.; Jin, C.; et al. *ACS Nano* **2016**, *10* (11), 10245.
(20) Chang, E. T.; Adami, H. O. *Cancer Epidemiol., Biomarkers Prev.* **2006**, *15* (10), 1765−1777.
(21) You, Y.; He, L.; Ma, B.; Chen, T. *Adv. Funct. Mater.* **2017**, *27* (42), 1703313.
(22) Pant, S.; Hilton, H.; Burczynski, M. E. *Biochem. Pharmacol.* **2012**, *83* (11), 1484−1494.
(23) Valadi, H.; Ekström, K.; Bossios, A.; Sjöstrand, M.; Lee, J. J.; Lötvall, J. O. *Nat. Cell Biol.* **2007**, *9* (6), 654.
(24) Wang, X.; Li, J.; Wang, Y.; Koenig, L.; Gjyrezi, A.; Giannakakou, P.; Shin, E. H.; Tighiouart, M.; Chen, Z. G.; Nie, S.; et al. *ACS Nano* **2011**, *5* (8), 6184.
(25) Fan, K.; Wang, H.; Xi, J.; Liu, Q.; Meng, X.; Duan, D.; Gao, L.; Yan, X. *Chem. Commun.* **2017**, *53* (2), 424.
(26) Balasubramanian, V.; Correia, A.; Zhang, H.; Fontana, F.; Mäkilä, E.; Salonen, J.; Hirvonen, J.; Santos, H. A. *Adv. Mater.* **2017**, *29* (11), 1605375.
(27) Fang, R. H.; Hu, C. M. J.; Luk, B. T.; Gao, W.; Copp, J. A.; Tai, Y.; O'Connor, D. E.; Zhang, L. *Nano Lett.* **2014**, *14* (4), 2181−2188.
(28) Hu, C.-M. J.; Zhang, L.; Aryal, S.; Cheung, C.; Fang, R. H.; Zhang, L. *Proc. Natl. Acad. Sci. U. S. A.* **2011**, *108* (27), 10980−10985.
(29) Shi, J.; Kundrat, L.; Pishesha, N.; Bilate, A.; Theile, C.; Maruyama, T.; Dougan, S. K.; Ploegh, H. L.; Lodish, H. F. *Proc. Natl. Acad. Sci. U. S. A.* **2014**, *111* (28), 10131−10136.
(30) Ding, H.; Lv, Y.; Ni, D.; Wang, J.; Tian, Z.; Wei, W.; Ma, G. *Nanoscale* **2015**, *7* (21), 9806−9815.

DOI: 10.1021/acs.nanolett.8b03709
Nano Lett. 2019, 19, 203−209

(31) Fu, Q.; Lv, P.; Chen, Z.; Ni, D.; Zhang, L.; Yue, H.; Yue, Z.; Wei, W.; Ma, G. *Nanoscale* **2015**, *7* (9), 4020−4030.

DOI: 10.1021/acs.nanolett.8b03709
Nano Lett. 2019, 19, 203−209